Supplementary information for: Experimental and theoretical optical properties of methylammonium lead halide perovskites

Aurélien M. A. Leguy[1*], Pooya Azarhoosh[2]*, M. Isabel Alonso[3], Mariano Campoy-Quiles[3], Oliver J. Weber[4], Jizhong Yao[1], Daniel Bryant[5,6], Mark T. Weller[4], Jenny Nelson[1,6], Aron Walsh[4], Mark van Schilfgaarde[2] and Piers R.F. Barnes[1†]

1- Physics department, Imperial College London, UK, SW7 2AZ;
2- Physics department, Kings College London, UK, WC2R 2LS;
3- Institut de Ciència de Materials de Barcelona (ICMAB-CSIC), Spain, 08193;
4- Chemistry department, University of Bath, UK, BA2 7AY;
5- Chemistry department, Imperial College London, UK, SW7 2AZ;
6- SPECIFIC, College of Engineering, Swansea University, Baglan Bay Innovation and Knowledge Centre, Central Avenue, Baglan, United Kingdom, SA12 7AX;

* Both authors equally contributed to the work.

‡ mark.van_schilfgaarde@kcl.ac.uk

† piers.barnes@imperial.ac.uk

List of the supplementary material as called in the main text:

Note S1 ***Detailed methods for sample preparation***

Methylammonium lead iodide single crystals were prepared according to the method of Poglitsch and Weber[1]. 2.5 g of lead acetate trihydrate ($Pb(CH_3CO_2)_2 \bullet 3H_2O$, Sigma 99.99 %) was dissolved in 10 mL hydroiodic acid (HI_{aq}, 57 wt%, Sigma) in a 50 mL round bottom flask and heated to 100 °C in an oil bath. Separately, 0.597 g of CH_3NH_2 (aq, 40 %, Sigma) was added dropwise to a further 2 mL of HI_{aq} kept at 0 °C in an ice bath under stirring. The methylammonium iodide solution was then added to the lead acetate solution and the mixture was cooled over five days to a temperature of 46 °C, resulting in the formation of black crystals with largest face length around 8 mm. The content of the flasks was subsequently filtered and dried for 12 hours at 100 °C.

Methylammonium lead bromide single crystals were prepared using 10 mL HBr (aq, 48 wt %, Sigma) was added to 1.458 g of $Pb(CH_3CO_2)_2.3H_2O$ in a 23 mL Teflon-lined stainless steel autoclave. Separately, 1 mL HBr was added dropwise to 0.333 mL of methylamine (aq, 40 %, Sigma) at 0 °C under stirring. The methylamine hydrobromide solution was then added to the autoclave, which was sealed and heated in a fan oven at 140 °C for 24 hours. The temperature was decreased from 140 °C to room temperature over five days. The red < 2mm crystals were filtered and dried for 12 hours at 100 °C.

Methylammonium lead chloride single crystals were prepared with 1.458 g $Pb(CH_3CO_2)_2.3H_2O$ and 3.892 g methylamine hydrochloride (Sigma)were added to a 23 mL Teflon-lined stainless steel autoclave along with 10 mL H_2O, affording a 15:1 molar ratio

$Pb(CH_3CO_2)_2.3H_2O$: MA.HCl. The reactants were heated in a fan oven at 140 °C for 24 hours. The temperature was decreased from 140 °C to room temperature over five days. The clear < 3 mm crystals were filtered and dried for 12 hours at 100 °C.

Methylammonium lead iodide thin films were prepared using methylammonium synthesized in advance by reacting 30 mL hydroiodic acid (57% in water, Aldrich) and 72 mL methylamine (33 % in ethanol, Aldrich) with 150ml ethanol in a 250mL round bottom flask for 2 h, with stirring. The precipitates were recovered by evaporation using rotary evaporator and further purified by dissolving in ethanol and recrystallized from diethyl ether followed by drying under vacuum.

A perovskite precursor solution was made by mixing a stoichiometric ratio of PbI_2 (Aldrich) and MAI which was dissolved in a mix of DMSO and GBL (7:3) and stirred for 10 minutes at 70°C. This perovskite precursor solution was coated onto glass substrates, previously cleaned using plasma cleaning, by a two-step spin coating procedure in a nitrogen glovebox environment to reduce the impact of oxygen and moisture. The spin coating procedure consisted of spinning the samples at 1000rpm for 20 seconds and then 4000rpm for 40 seconds. During the second step toluene was dripped onto the surface to initial crystallisation as reported previously.[2] Samples were then dried at 100°C for 10minutes on a hot plate.

Perovskite devices were fabricated by infiltrating a mesoporous Al_2O_3 layer with $MAPbI_3$. Fluorine-doped tin oxide (FTO) coated glass was used as substrate. Samples were cleaned in detergent, acetone, and ethanol before a 10 min oxygen plasma treatment. A 50 nm compact layer of TiO_2 was deposited by spray pyrolysis at 450 °C. The mesoporous Al_2O_3 film was obtained by spin-coating a dispersion of Al_2O_3 nanoparticles onto the samples and subsequent drying at 150 °C. The infiltration and capping layer of $MAPbI_3$ was prepared from solution by mixing PbI_2 (Sigma-Aldrich) with MAI (1:1 molar ratio) in a mixture of GBL and DMSO (7:3 v/v) at 70°C for 12 h. The mixture was then filtrated with 0.2 μm syringe filters (PTFE, VWR). The solution was spin-coated onto the alumina scaffold by a consecutive two-steps spin-coating process at 1,000 and 4,000 r.p.m for 10 and 50 s, respectively. During the second spin-coating step, the substrate (around 12 mm × 12 mm) was treated with toluene drop-casting. The hole transport layer was deposited by spin-coating a 7.7wt% solution of 2,2',7,7'-tetrakis-(N,N-di-pmethoxyphenylamine)9,9-spirobifluorene (spiro-OMeTAD, Lumtec) in chlorobenzene with added 4-tert-butylpyridine (tBP) and lithium

bis(trifluoromethanesulfonyl)imide (Li-TFSI) onto the sample. Devices were completed by evaporating Au contact electrodes through a shadow mask.

Note S2 ***Method for measuring sub-band gap external quantum efficiency***

EQE was measured using a grating spectrometer (CVI DIGIKROM 240) to create monochromatic light combined with a tungsten halogen light source. The monochromatic light was chopped at 235 Hz and Stanford Research Systems SR380 lock-in amplifier with an internal transimpedance amplifier of 10^6 V/A was used to detect the photocurrent. Long pass filters at 610, 715, 780, 850, and 1000 nm were used to filter out higher order diffracted and scattered light from monochromator. The spectra were taken from 350 to 1100 nm and calibrated by a silicon photodiode.

Note S3 ***Method for measuring diffuse Reflectance***

Diffuse reflectance measurements were performed with a Shimadzu UV-2600 spectrometer equipped with an integrating sphere. Samples composed of a weight ratio of 50 % $BaSO_4$ powder and 50 % MAPbX_3 single crystals crushed into a fine powder. The Kubelka-Munk function was used for quantitative analysis: $F(R_{inf}) = (1 - R_{inf})^2/2\ R_{inf}$ where R_{inf} is the ratio of diffuse scattered light by a thick layer of the sample over the light scattered from the standard reference powder ($BaSO_4$). The intercept of the tangent of the inflexion point of ($h\nu$*$F(R_{inf})$) vs $h\nu$ with the x-axis on the Tauc plots was used to estimate of the bandgaps. $F(R_{inf})$ was assumed to be approximately proportional to the absorption coefficient, (α) which is reasonable if the scattering coefficient of the powder mixture is relatively constant.[3] This data was geometrically rescaled so that absorption shoulder matched amplitude of the non-excitonic shoulder of the absorption coefficient derived from the ellipsometry data near the band edge.

Note S4 ***Details of the fitting procedure***

The dielectric function is then calculated from the CP model, which enables the software to simulate spectrometric values of ψ and Δ at the angles of incidence used for the acquisition via transfer matrix calculations. For optically isotropic samples, these parameters relate to the Fresnel coefficients R_p and R_s for p- and s- polarized light:

$$\frac{R_p}{R_s} = \tan(\psi)\, e^{i\Delta} \qquad (1)$$

Finally, a regression algorithm fits the generated curve to the experimental one by varying the free parameters (for example: the layer thickness and the amplitude or energy centre of an oscillator). The figure of merit quantifying the quality of the fits is the mean square error (MSE), given by:

$$MSE = \sqrt{\frac{1}{2N'-M}\sum_{i=1}^{N'}\left[\left(\frac{\Psi_i^{\mathrm{mod}}-\psi_i^{\mathrm{exp}}}{\sigma_{\psi,i}^{\mathrm{exp}}}\right)^2+\left(\frac{\Delta_i^{\mathrm{mod}}-\Delta_i^{\mathrm{exp}}}{\sigma_{\Delta,i}^{\mathrm{exp}}}\right)^2\right]} \quad (2)$$

N' is the number of (ψ,Δ) pairs, M the number of variable parameters in the model and σ the standard deviations on the experimental data points.

Note S5 ***The Bruggeman approximation***

The Bruggeman approximation is an analytical averaging method commonly used to study the macroscopic properties of composite materials. In the case of ellipsometry modelling, the approximation is used to estimate the optical constants of two (or more) intimately mixed phases. It assumes homogenous dispersion of one phase into another resulting into an effective medium (EMA). The effective dielectric function $\tilde{\varepsilon}$ of a material composed of two constituents A and B (with respective volume fractions f_A and f_B) can thus be written:

$$f_A\frac{\tilde{\varepsilon}_A-\tilde{\varepsilon}}{\tilde{\varepsilon}_A-2\tilde{\varepsilon}} = -f_B\frac{\tilde{\varepsilon}_B-\tilde{\varepsilon}}{\tilde{\varepsilon}_B-2\tilde{\varepsilon}} \quad (3)$$

This transcendental equation, also referred to as coherent potential approximation, is solved numerically for $\tilde{\varepsilon}$. In this work the layer roughness of $MAPbI_3$ thin films is modelled by an EMA with identical volume proportion of both the top layer and voids.[4]

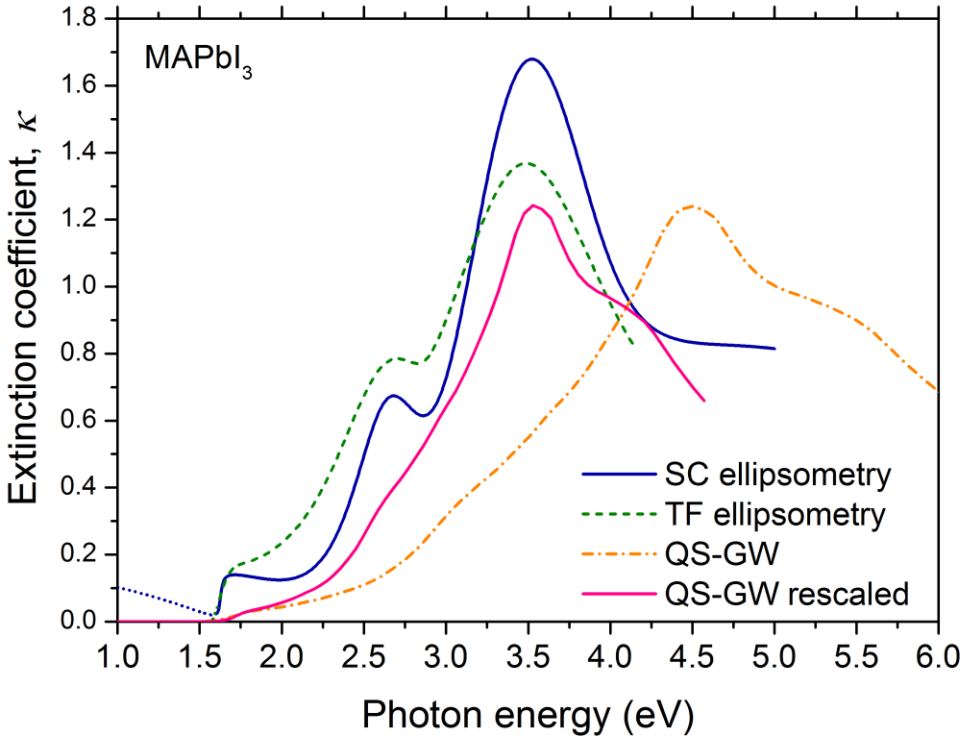

Figure S1 Calculated optical constants when the QS-GW results are rescaled using hν -> 0.653hν + 0.608 (solid pink line). The results from **Figure 2a** of the main text are reproduced for comparison. 'SC' stands for 'single crystal' and 'TF' for 'thin film'.

Note S6 ***Critical points vs harmonic oscillators:*** In literature, the most common approach to model the dielectric function of a material is to use an ensemble of harmonic oscillators (HO). This model, if appropriate to describe elementary electronic transitions in atoms, is often too rigid to characterize crystalline structures. The main limitation of harmonic oscillators, *i.e.* Lorentz or Gaussian, is that they describe perfectly symmetrical transitions.[5] The description of asymmetrical line shapes is only possible by 'pairing' two oscillators together, one with positive and one with negative amplitude. This forbids any meaningful interpretation of the oscillators as optical transitions; since more oscillators are required than optical transitions in the material.

Herein we use critical points (CPs) of the joint density of state (*jDOS*) as an alternative to HO. Only five CPs are required to satisfactorily describe the optical properties of MAPI – against 6 when HO are used –, each CP describing a 'physical' electronic transition. This allows a better definition of the energy centre of the optical features. The mathematical forms of both HO and CPs fulfil Kramers-Kronig relations.

Note that the phase parameter (see **Table S1 to S4**) of the bandgap excitation (as well as for some higher energy transitions) is not zero, which means that the transition results in an asymmetric (Fano) shape in the optical constants.[6] This type of profile is expected in case of interaction between a discrete excitation and a continuous background – here between the excitonic level and the *jDOS* continuum.[7, 8]

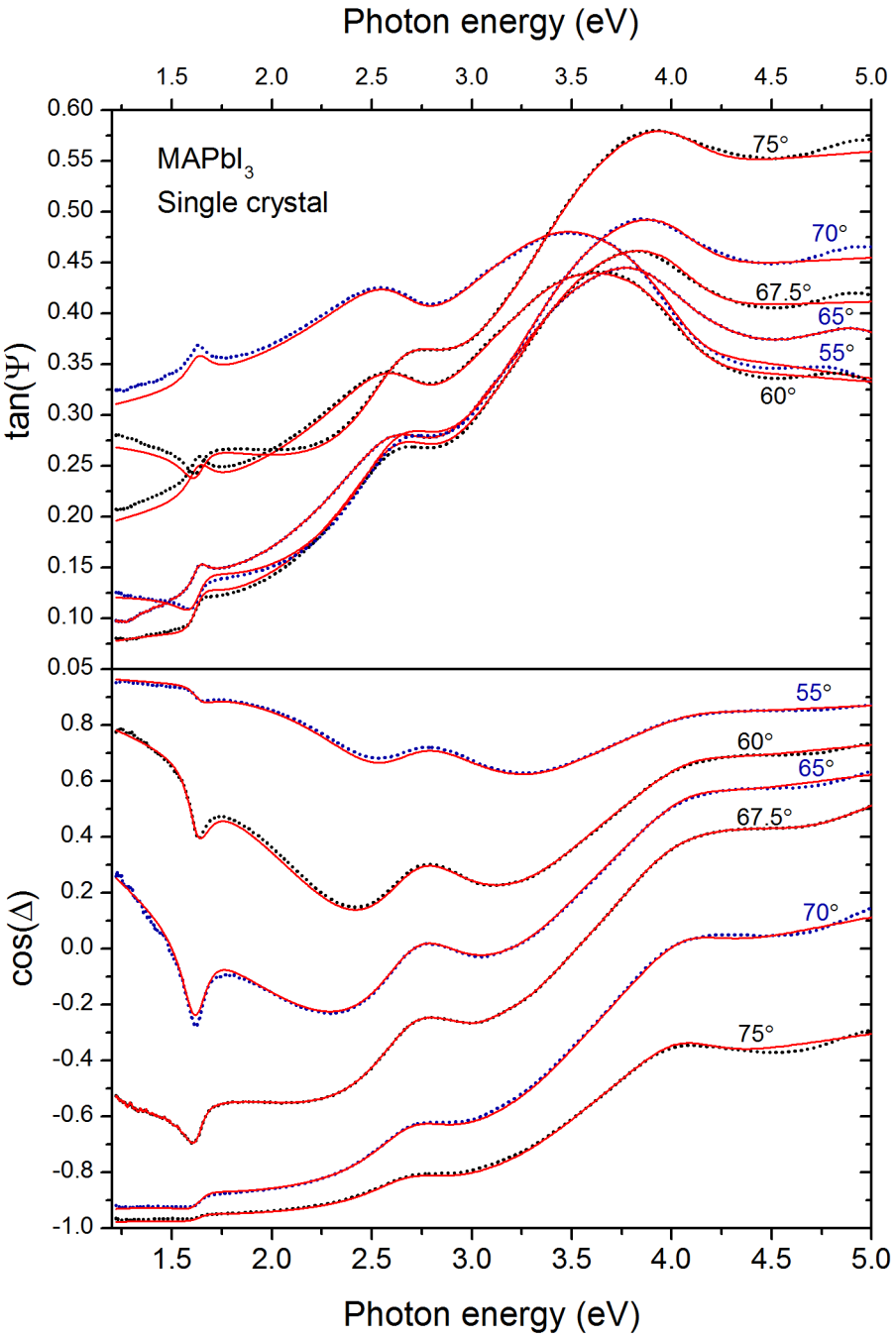

Figure S2 Fit of the ellipsometry parameters for $MAPbI_3$ single crystals. Spectroscopic curves of the ellipsometry parameters ψ and Δ have been acquired at 6 different angles of incidence on the 1.2 – 5 eV energy range. The dotted lines (blue or black) are the

experimental results while the solid red lines show the fits. The critical point model used for the fits is given in **Table S1**.

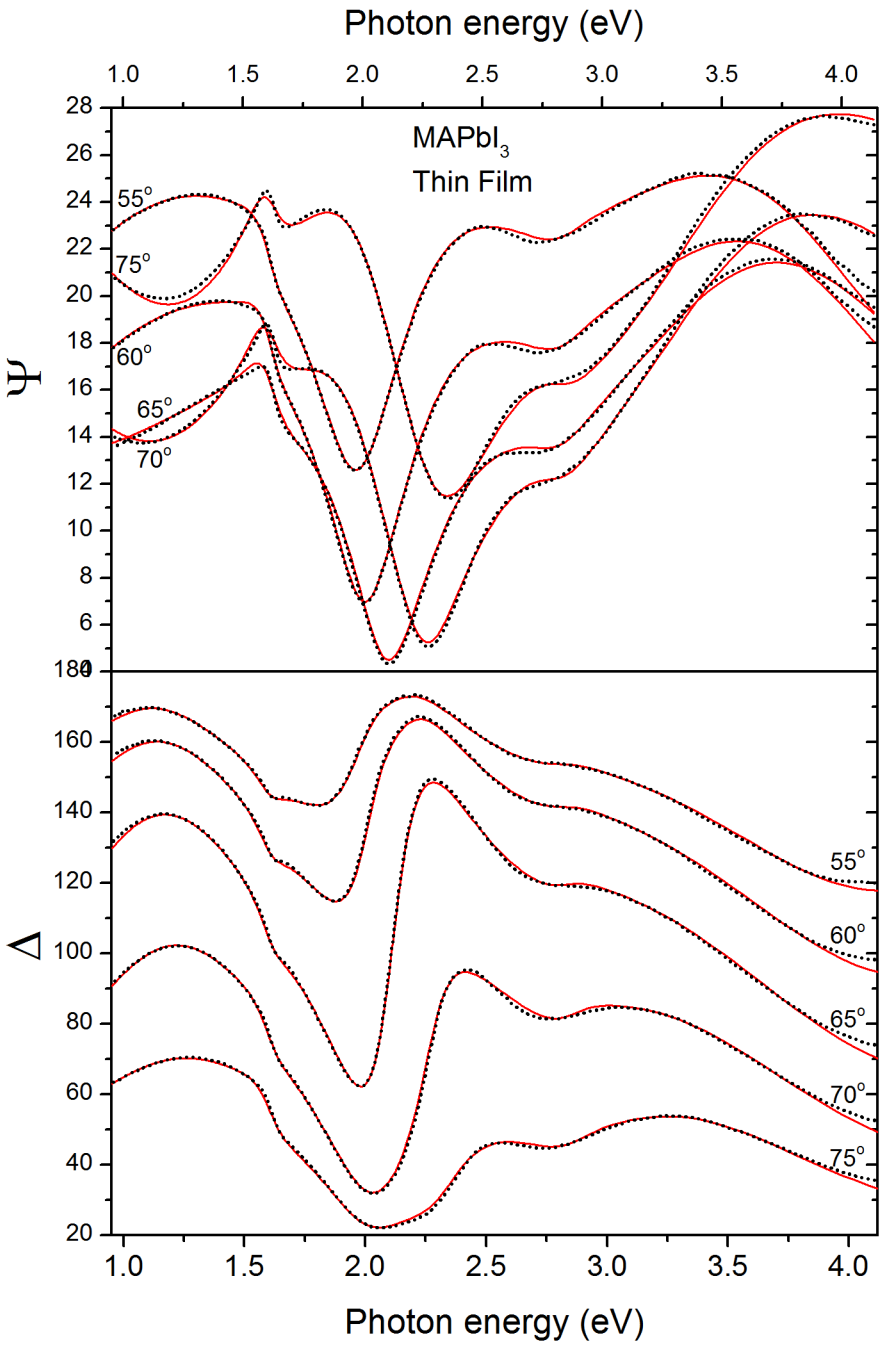

Figure S3 Typical fit of the ellipsometry parameters for a $MAPbI_3$ thin film. Spectroscopic curves of the ellipsometry parameters ψ and Δ have been acquired at 5 different angles of incidence on the 0.9 – 4.2 eV energy range. The black dotted lines are the experimental results while the solid red lines show the fits. The critical point model used for the fits is given in **Table S4**.

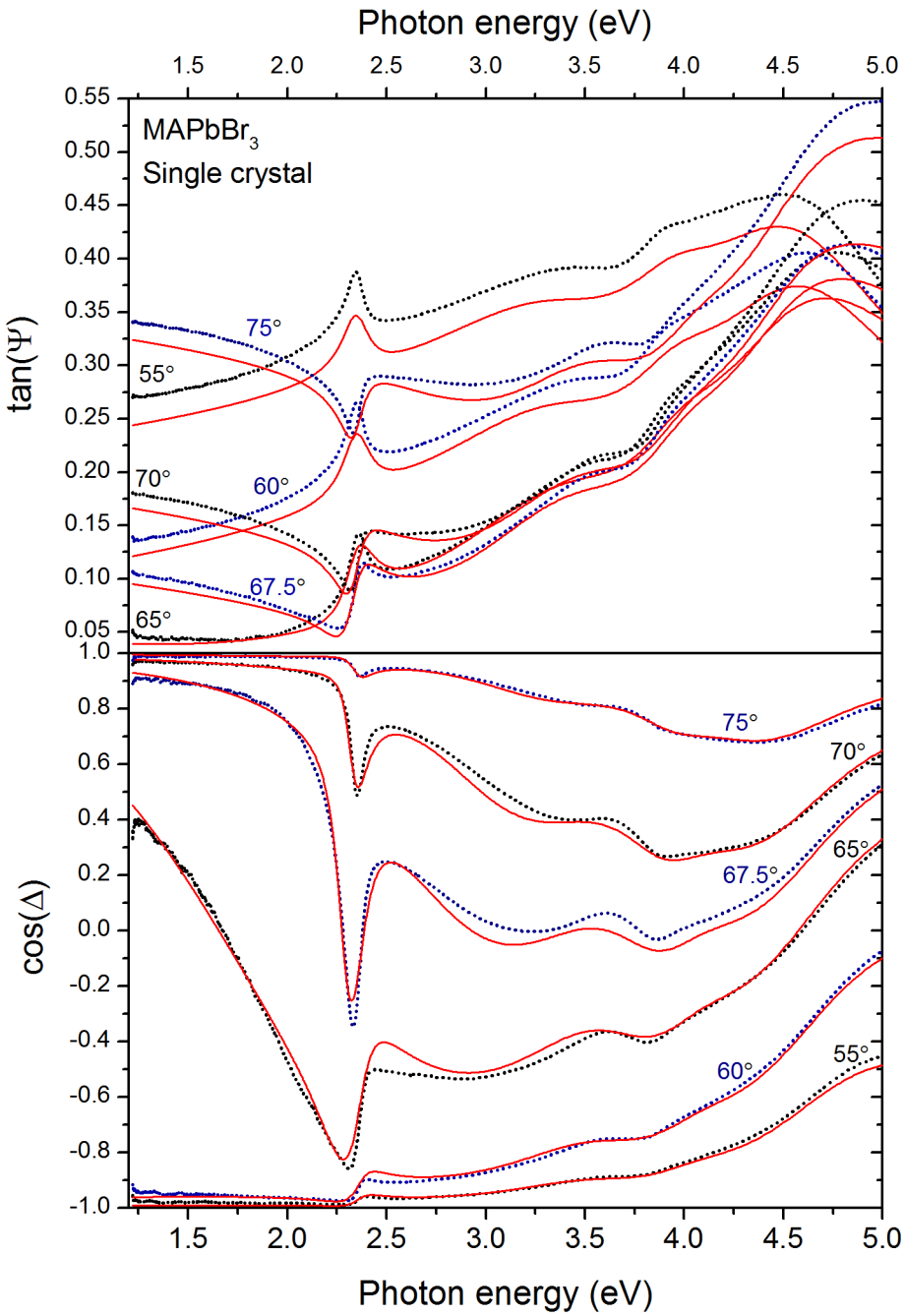

Figure S4 Fit of the ellipsometry parameters for $MAPbBr_3$ single crystals. Spectroscopic curves of the ellipsometry parameters ψ and Δ have been acquired at 6 different angles of incidence on the 1.2 – 5 eV energy range. The dotted lines (blue or black) are the experimental results while the solid red lines show the fits. The critical point model used for the fits is given in **Table S2**.

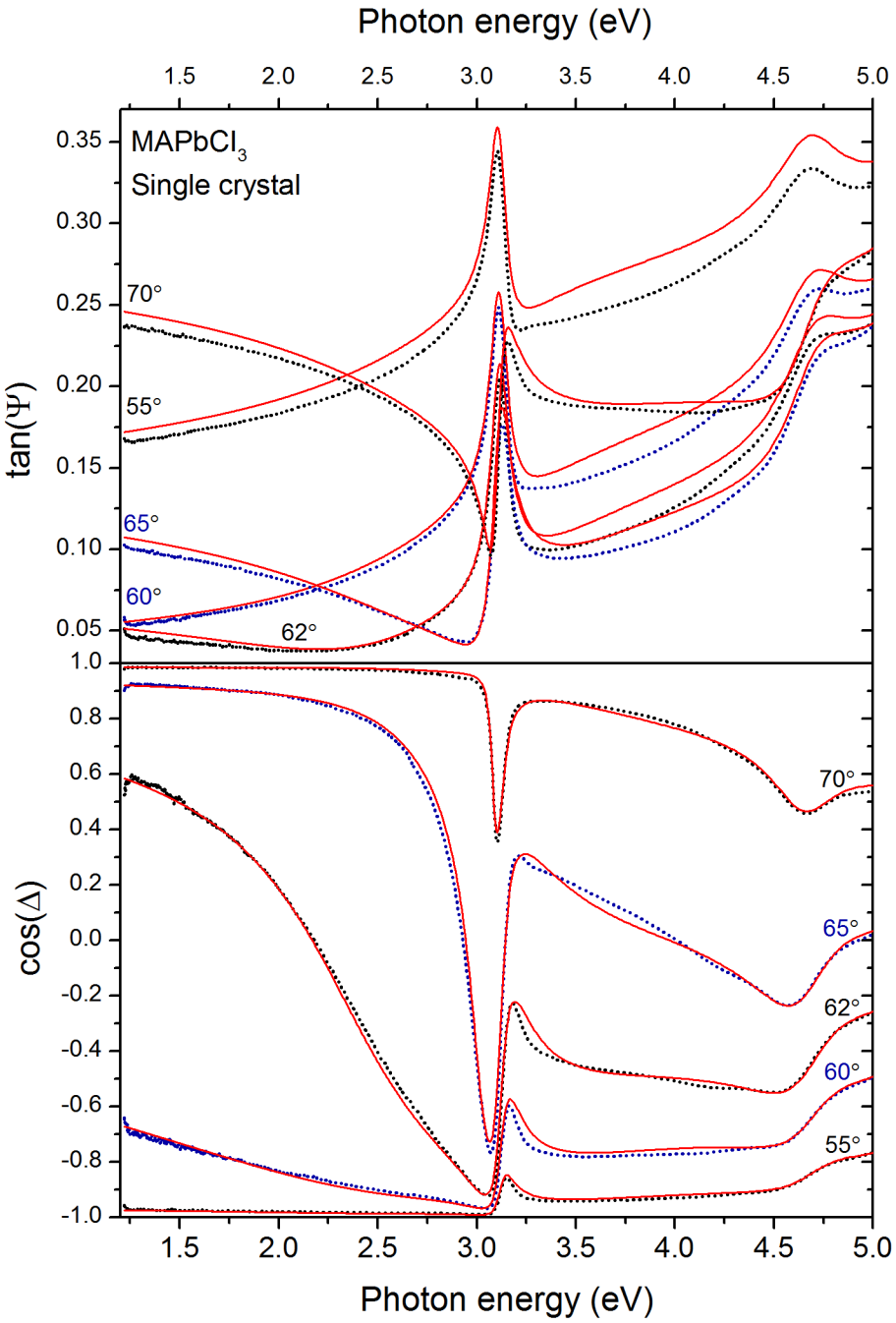

Figure S5 Fit of the ellipsometry parameters for $MAPbCl_3$ single crystals. Spectroscopic curves of the ellipsometry parameters ψ and Δ have been acquired at 6 different angles of incidence on the 1.2 – 5 eV energy range. The dotted lines (blue or black) are the experimental results while the solid red lines show the fits. The critical point model used for the fits is given in **Table S3**.

Table S1 Critical point model of $MAPbI_3$ single crystals obtained for the best fit of the ellipsometry parameters.

Critical point	Amplitude (F/m)	Phase (rad)	Energy centre (eV)	Broadening (eV)
1	0.041	-1.769	1.62	0.0673
2	0.67	-0.56	2.55	0.246
3	2.46	-0.399	3.31	0.32
4	0.3	-0.773	4.55	0.4
5	182	-1.15	10	44

Table S2 Critical point model of $MAPbBr_3$ single crystals obtained for the best fit of the ellipsometry parameters.

Critical point	Amplitude (F/m)	Phase (rad)	Energy centre (eV)	Broadening (eV)
1	0.072	-1.32	2.34	0.059
2	1.77	0.052	3.52	0.55
3	1.23	-1.44	3.88	0.37
4	0.728	-0.125	4.46	0.329
5	85	0.065	28	3

Table S3 Critical point model of $MAPbCl_3$ single crystals obtained for the best fit of the ellipsometry parameters.

Critical point	Amplitude (F/m)	Phase (rad)	Energy centre (eV)	Broadening (eV)
1	0.079	-0.765	3.11	0.033
2	0.651	-2.27	3.15	1.07
3	0.27	-0.858	4.64	0.234
4	1.22	0.617	5.59	0.58
5	85	0.068	27.7	2.11

Table S4 Critical point model of $MAPbI_3$ thin films obtained for the best fit of the ellipsometry parameters. The fitted functional in this case is $A_i e^{j\varphi}\left({\Gamma_i}/{2E_n - 2E - j\Gamma_i}\right)^{\mu}$, μ is the dimentionality $\mu = 1$ here for 0D CPs, Γ is the broadening, φ the phase, and *i* designates the critical point.

Critical point	Amplitude (F/m)	Phase (rad)	Energy centre (eV)	Broadening (eV)
1	0.732	-1.75	1.61	0.183
2	2.27	-0.616	2.5	0.815
3	1.2	-3.32	2.85	0.439
4	5.08	0.186	3.38	1.1
5	4.5	-0.788	6.97	10

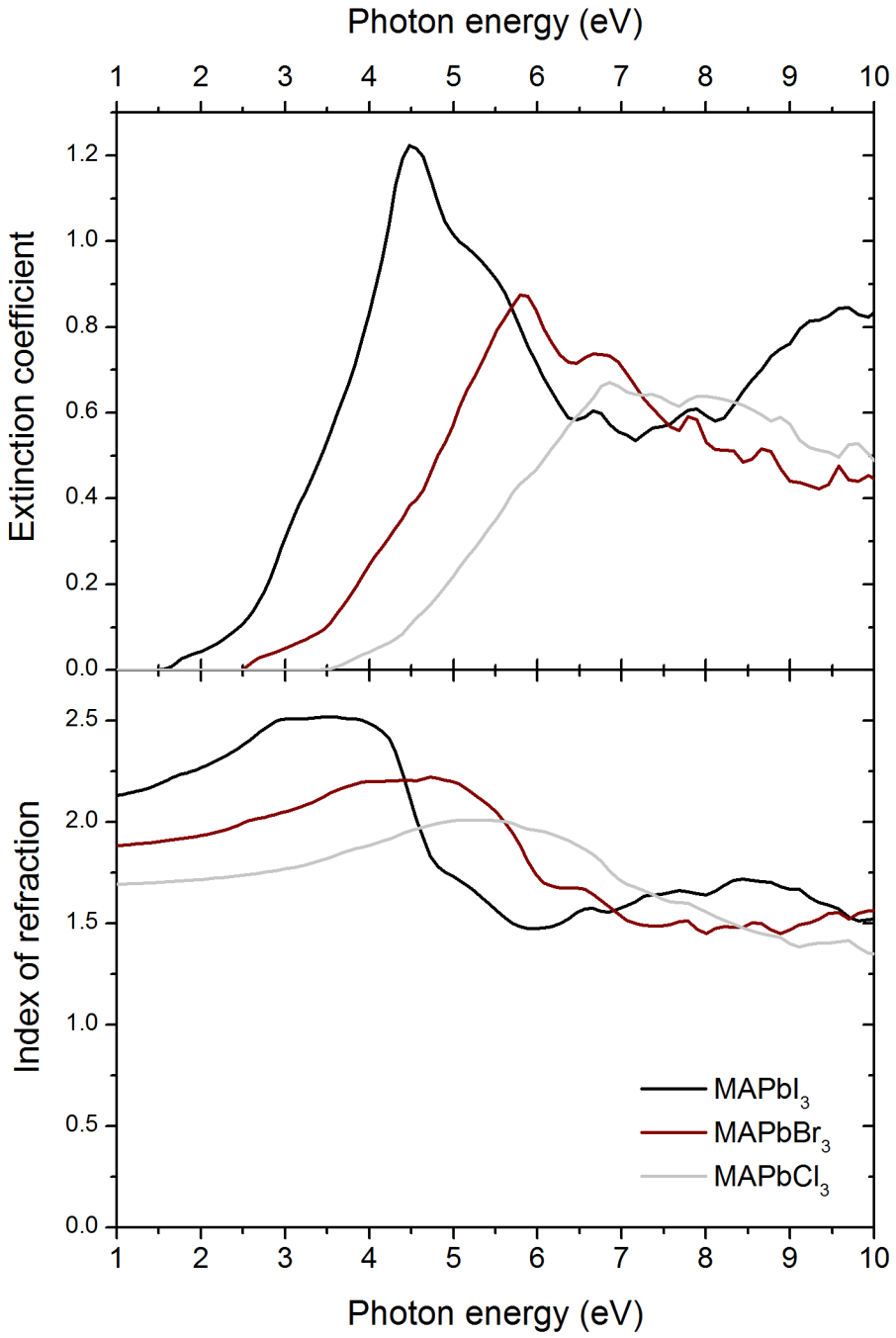

Figure S6 Optical constants (extinction coefficient (top) and index of refraction (bottom)) obtained in the QS-GW framework on the extended 1 – 10 eV energy range for the three compounds: $MAPbI_3$ (solid black line), $MAPbBr_3$ (solid brown line) and $MAPbCl_3$ (solid grey line).

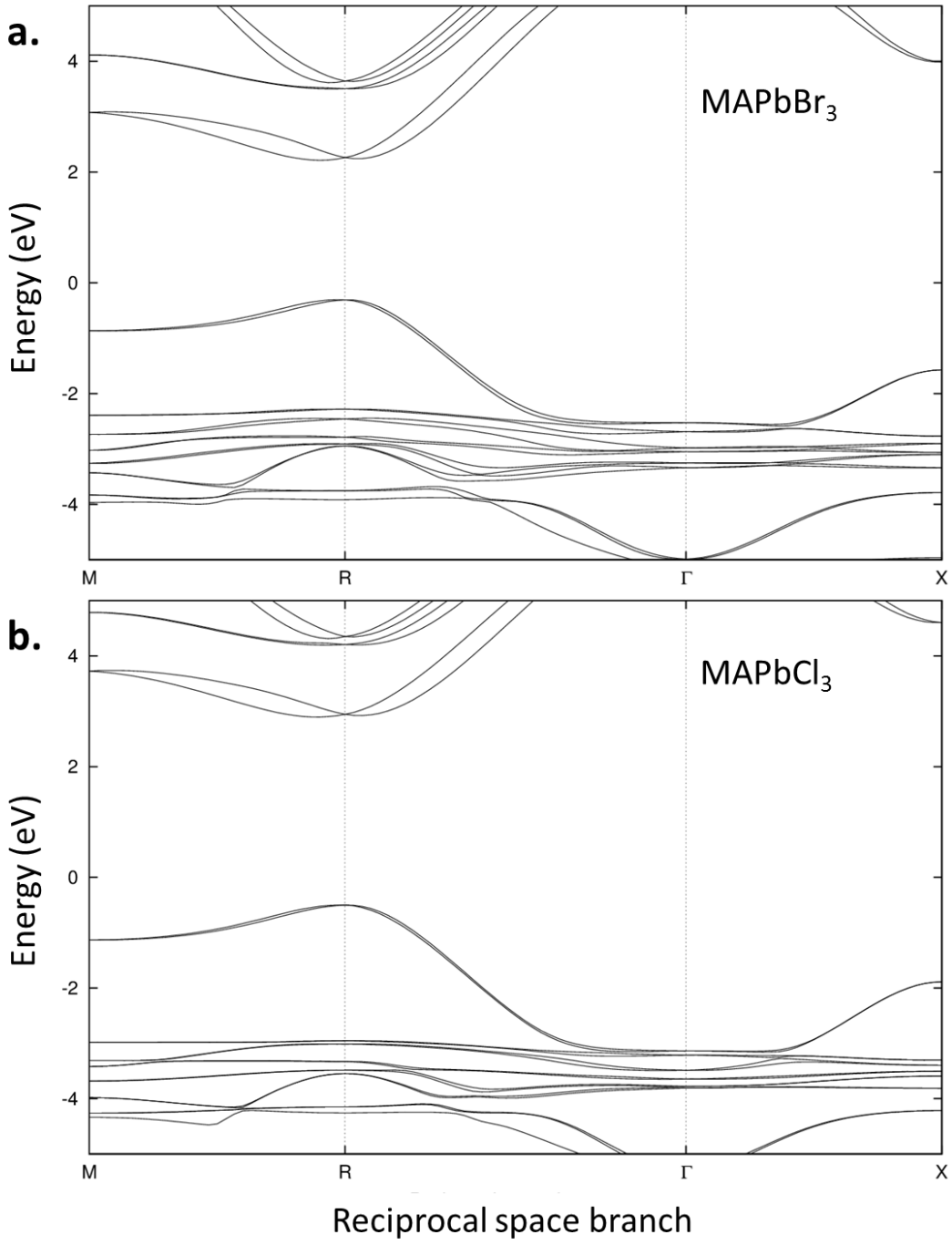

Figure S7 Energy band diagram of $MAPbBr_3$ (**a.**) and $MAPbCl_3$ (**b.**) along the relevant k-branches in the first Brillouin zone. The labels tag the critical point transitions with the appropriate inter-band transitions (see **Figure 2** in the **main text**)

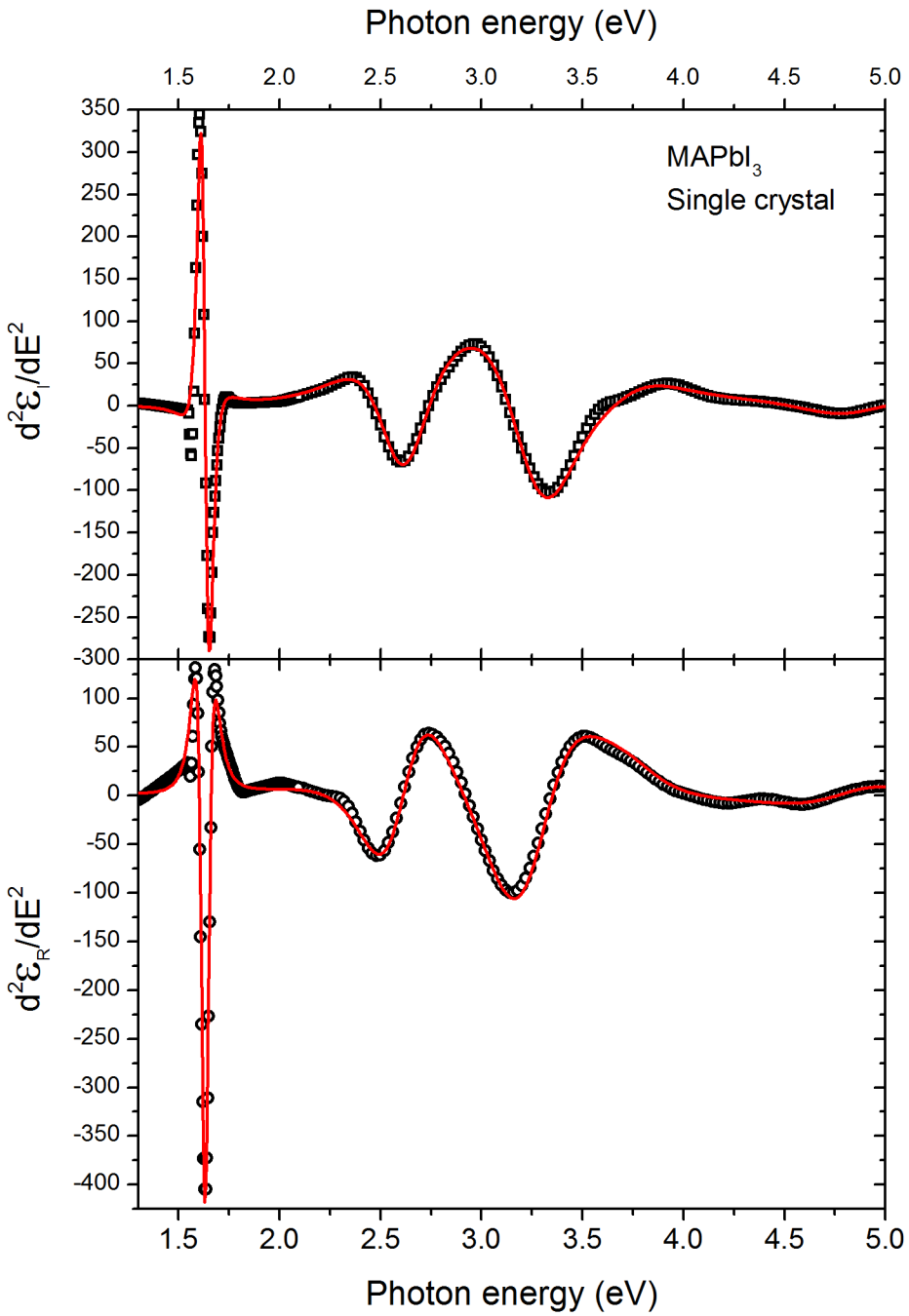

Figure S8 Fit of $d^2\varepsilon/dE^2$ for $MAPbI_3$ single crystals. The experimental data is plotted using black markers, while the fit is represented by the solid red line. The functional used for the fit is given in the main text, in the methods section. The critical point model obtained for the best fit is given in **Table S5**.

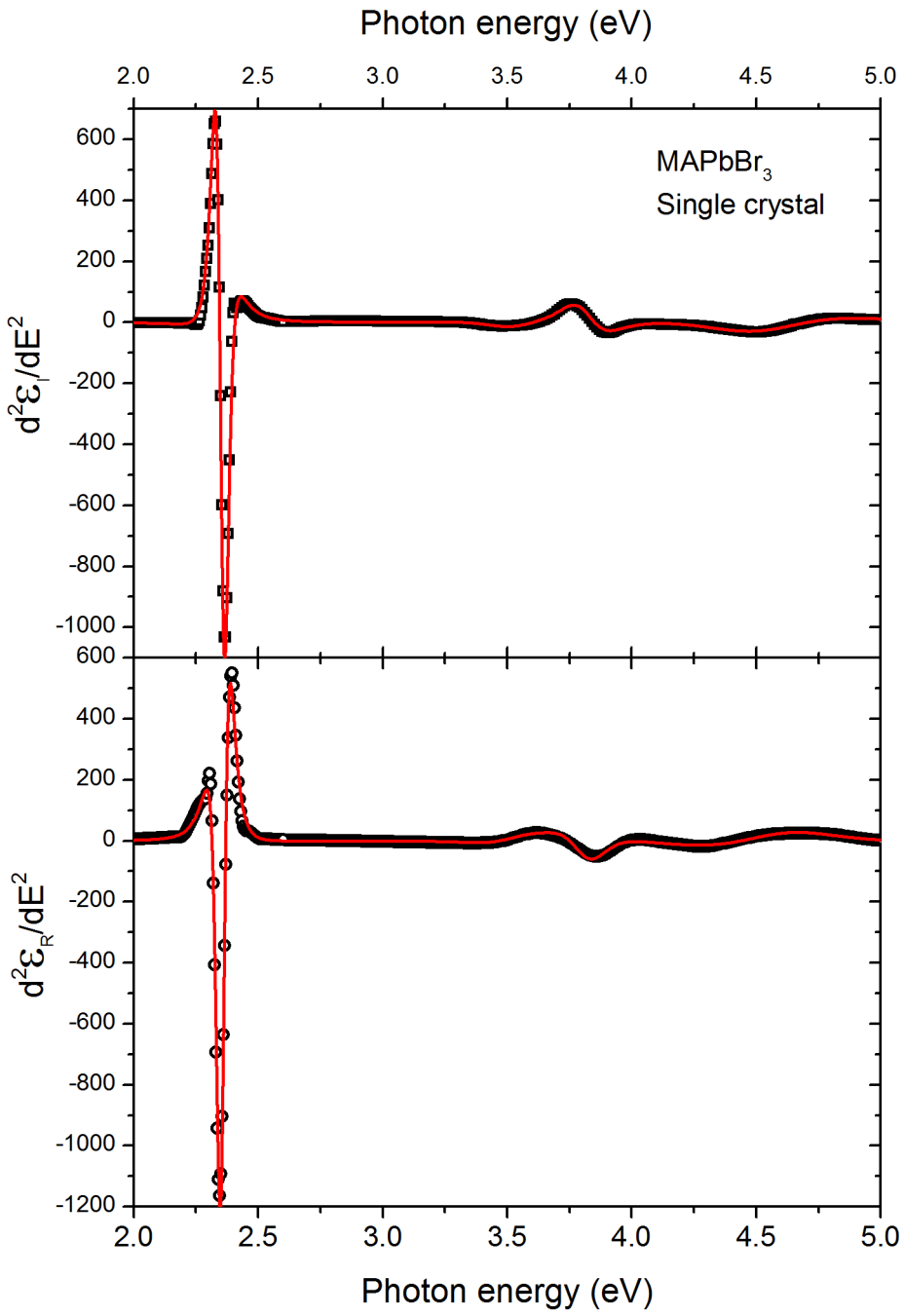

Figure S9 Fit of $d^2\varepsilon/dE^2$ for $MAPbBr_3$ single crystals. The experimental data is plotted using black markers, while the fit is represented by the solid red line. The functional used for the fit is given in the main text, in the methods section. The critical point model obtained for the best fit is given in **Table S6**.

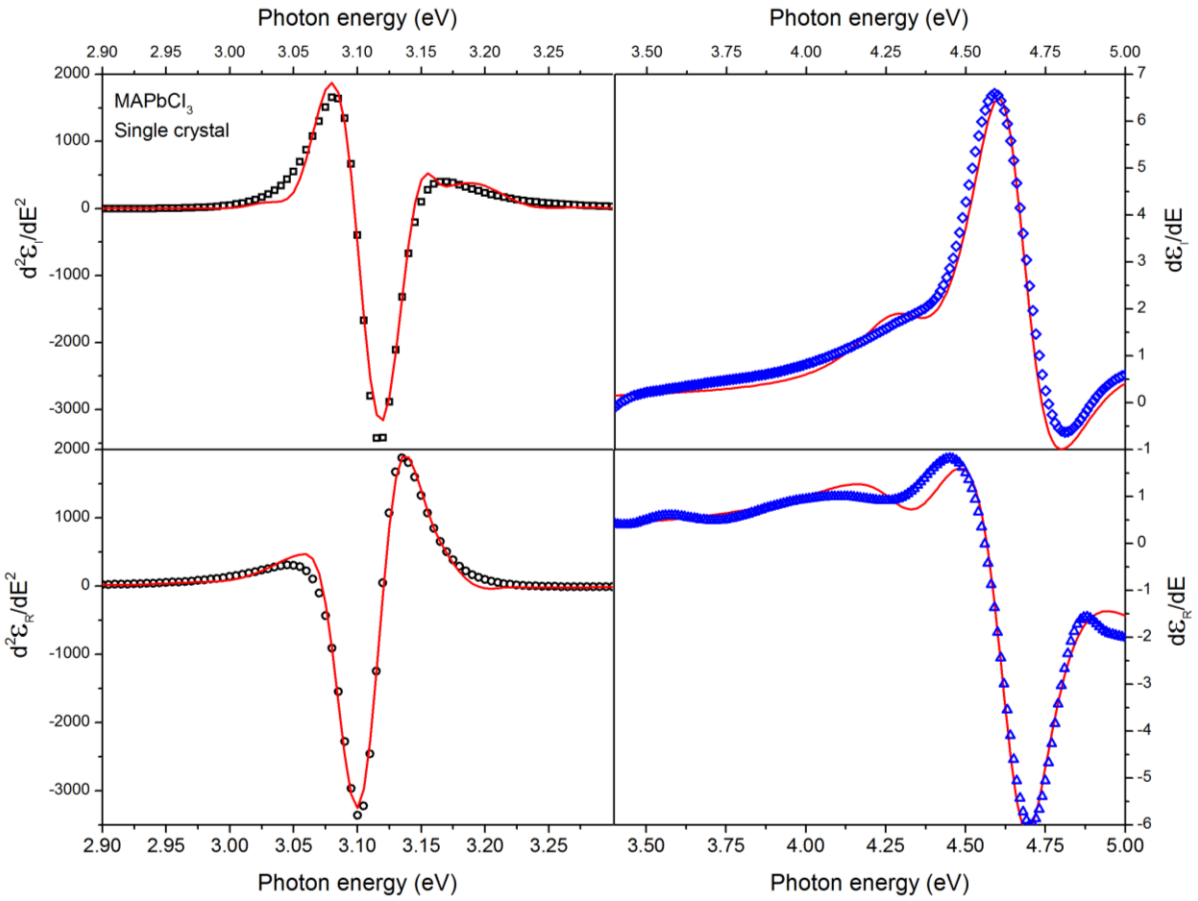

Figure S10 Fit of $d^2\varepsilon/dE^2$ and $d\varepsilon/dE$ for $MAPbCl_3$ single crystals. $d\varepsilon/dE$ is fitted for the higher energy critical points because fits of $d^2\varepsilon/dE^2$ were not conclusive on this range. The experimental data is plotted using black ($d^2\varepsilon/dE^2$) or blue ($d\varepsilon/dE$) markers, while the fits are represented by solid red lines. The functional used for the fit is given in the main text, in the methods section. The critical point model obtained for the best fit is given in **Table S7**.

Table S5 Critical point model of $MAPbI_3$ obtained by fitting the ellipsometry the second derivative of the dielectric function $d^2\varepsilon/dE^2$.

Critical point	Amplitude ($Fm^{-1}eV^{-2}$)	Phase (rad)	Energy centre (eV)	Broadening (eV)
1	0.028	-1.68	1.63	0.051
2	1.2	-0.192	2.6	0.302
3	4.16	-0.628	3.26	0.415
4	0.44	1.22	3.69	0.406
5	0.9	0.524	4.84	0.539

Table S6 Critical point model of $MAPbBr_3$ obtained by fitting the ellipsometry the second derivative of the dielectric function $d^2\varepsilon/dE^2$.

Critical point	Amplitude ($Fm^{-1}eV^{-2}$)	Phase (rad)	Energy centre (eV)	Broadening (eV)
1	0.06	-1.01	2.35	0.0455

2	0.08	0.628	3.54	0.233
3	0.14	-2.09	3.81	0.171
4	1.77	0.663	4.55	0.487

Table S7 Critical point model of $MAPbCl_3$ obtained by fitting the ellipsometry the second derivative of the dielectric function $d^2\varepsilon/dE^2$ (CP1) and the first derivative $d\varepsilon/dE$ (CP2 to 4).

Critical point	Amplitude ($Fm^{-1}eV^{-2}$)	Phase (rad)	Energy centre (eV)	Broadening (eV)
1	0.12	-0.698	3.11	0.0401
2	0.05	-0.611	4.34	0.2
3	0.18	-0.611	4.66	0.169
4	1.35	-0.0698	5.27	0.705

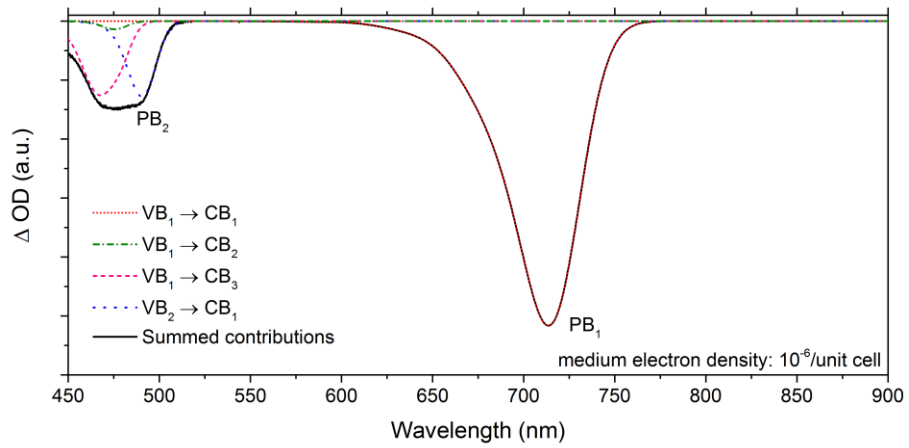

Figure S11 Simulated transient absorption spectrum for a charge carrier density of 10^{-6} per unit cell. The dashed black line corresponds to the summed contribution of all transitions and rescaled according to the procedure detailed in the **methods section**. The main individual contributions are shown (solid coloured lines). 'PB1' and 'PB2' label the two photo-bleaches.

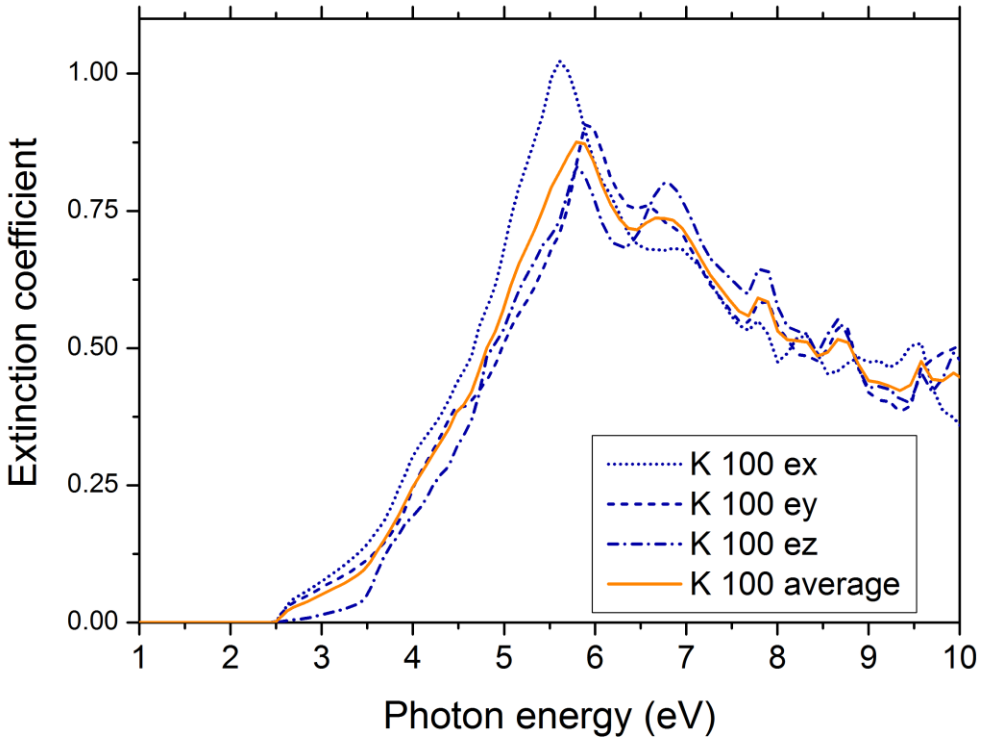

Figure S12 Anisotropy of calculated optical constants of $MAPbBr_3$ in the three directions of space (ex, ey and ez).The equilibrium orientation is assumed to correspond to MA^+ pointing at the faces of the cube formed by the surrounding lead atoms (direction <100>).

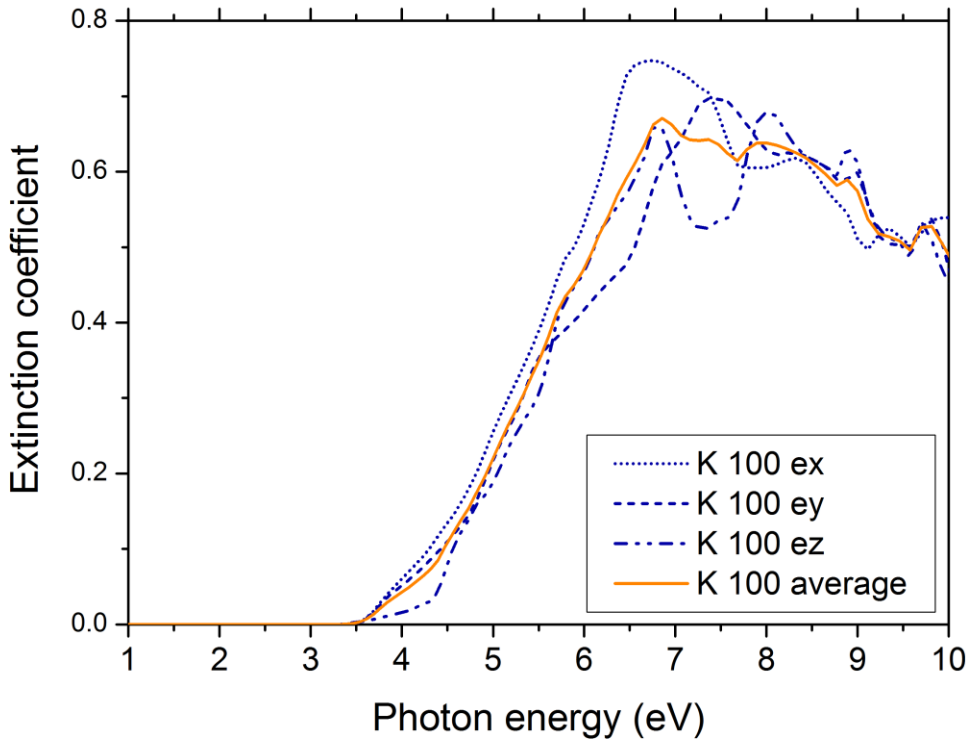

Figure S13 Anisotropy of calculated optical constants of $MAPbCl_3$ in the three directions of space (ex, ey and ez).The equilibrium orientation is assumed to correspond to MA^+ pointing at the faces of the cube formed by the surrounding lead atoms (direction <100>).

Biliography:

1. A. Poglitsch and D. Weber, *The Journal of Chemical Physics*, 1987, **87**, 6373-6378.
2. Z. Xiao, Q. Dong, C. Bi, Y. Shao, Y. Yuan and J. Huang, *Advanced Materials*, 2014, **26**, 6503-6509.
3. E. M. Patterson, C. E. Shelden and B. H. Stockton, *Applied Optics*, 1977, **16**, 729-732.
4. H. Fujiwara, J. Koh, P. I. Rovira and R. W. Collins, *Physical Review B*, 2000, **61**, 10832-10844.
5. M. Campoy-Quiles, J. Nelson, D. D. C. Bradley and P. G. Etchegoin, *Physical Review B*, 2007, **76**, 235206.
6. U. Fano, *Phys. Rev.*, 1961, **124**, 1866--1878.
7. P. Lautenschlager, M. Garriga, S. Logothetidis and M. Cardona, *Phys. Rev. B*, 1987, **35**, 9174--9189.
8. P. Lautenschlager, M. Garriga, L. Vina and M. Cardona, *Phys. Rev. B*, 1987, **36**, 4821--4830.